DOI:10.1039/C1JM12426A (Paper) *J. Mater. Chem.*, 2011, **21**, 15218-15223

Nanorod decorated nanowires as highly efficient SERS-active hybrids

Ramesh Kattumenu [a], **Chang H. Lee** [a], **Limei Tian** [a], **Michael E. McConney** [b] **and Srikanth Singamaneni** *[a]

[a]*Department of Mechanical Engineering and Materials Science, Washington University, St. Louis, MO 63130. E-mail: singamaneni@wustl.edu*

[b]*Materials and Manufacturing Directorate, Air Force Research Laboratory, Wright-Patterson Air Force Base, OH 45433*

Received 30th May 2011 , Accepted 11th July 2011

First published on the web 8th August 2011

In order to propel surface enhanced Raman scattering (SERS)-based sensing into the real world, novel SERS-active nanostructure designs that enable facile, scalable, cost-effective, highly efficient and homogenous SERS substrates are paramount. We demonstrate the facile fabrication of highly efficient SERS-active 3D nanohybrids based on vertically aligned zinc oxide nanowires uniformly decorated with gold nanorods. The dramatic enhancement of the surface area (nearly 20 times) and hence the number of plasmonic nanostructures within the incident laser foot print results in more than *three orders of magnitude* increase in SERS intensity compared to planar SERS substrates. The SERS enhancement factor was found to be $\sim 3 \times 10^7$ with a detection limit of sub-pM for a non-resonant analyte. Apart from excellent sensitivity, the nanohybrids also exhibited excellent lateral and vertical homogeneity in SERS activity. We believe that under optimal conditions these nanohybrids can surpass the best 2D substrate designs in SERS enhancement and homogeneity.

Introduction

Surface enhanced Raman scattering (SERS), which involves the dramatic enhancement of Raman scattering from an analyte adsorbed on or in close proximity to a nanostructured metal surface, is a rapidly emerging tool for trace chemical and biological detection, enviromental monitoring and homeland security.[1–5] Numerous SERS substrates, from roughened metal films to highly ordered nanostructure assemblies fabricated using e-beam lithography have been designed and tested for the trace level monitoring of chemical and biological analytes.[6] 1D SERS substrates, which include nanoparticle and nanodisk strings,[7–11] and 2D SERS substrates comprised of densely-packed nanoparticles and their periodic arrays obtained by nanosphere lithography and Langmuir–Blodgett assembly have been extensively investigated as SERS substrates.[12–16] 3D SERS substrates, which can be characterized as open metal/hybrid nanostructures providing light interaction with the whole structure, such as nanocanal arrays decorated with metal nanoparticles, metallic nanohole arrays, microstructured optical fibers decorated with metal nanoparticles and nanoporous metallic membranes, offer the advantage of large specific surface area with high number of plasmonic nanostructures (and hot spots) within the laser footprint.[6,17–25]

General strategy of 3D SERS substrates involves the uniform decoration of the 3D templates with plasmonic nanostructures. One of the common challenges with most 3D substrates demonstrated so far is acheiving uniform distribution of the plasmonic nanostructures over the entire template.[26] The use of conventional deposition techniques like vacuum infiltration, immersion plating and electrochemical deposition, results in pore clogging, non-uniform distribution of the plasmonic nanostructures and poor control over the size and shape of the metal nanostructures that can be deposited within the pores of the 3D templates, thereby producing non-uniform SERS substrates with poor reproducibility.[27] Major improvements in the performace of 2D SERS substrates have been acheived by precise control of the size, shape and assembly of the plasmonic nanostructures.[6] Similar control over the size, shape and assembly in conjunction with facile and cost-effective fabrication of 3D templates is extremely important to achieve highly sensitve 3D SERS substrates for trace detection of chemical and biological species.

Zinc oxide (ZnO) is a wide bandgap semiconducting material that has attracted much interest due to its unique optical and electrical properties as a typical metal oxide semiconductor material.[28–30] In addition to the applications relying on the semiconducting and piezoelectric properties of ZnO, another potential application that has been gaining importance is SERS.[31–33]

ZnO nanowires (ZnO NW) are promising candidates for the fabrication of 3D SERS substrates due to their facile synthesis and tunability of the morphology, large surface to volume ratio, and optical transparency. Numerous morphologies such as wires, belts (ribbons), rings, flowers, propellers, cages have been fabricated using solution and vapor phase methods.[34–39]

In this work, we report a highly sensitve and uniform 3D SERS substrate based on solution grown ZnO NW decorated with gold nanorods (AuNR). The SERS substrate was prepared by the chemical bath deposition of vertically aligned ZnO NW on a large area silicon substrate. The high aspect ratio ZnO nanowires decorated with AuNR result in a large increase in the number of AuNR within the incident laser footprint thus dramatically enhacing the SERS intensity. The SERS substrate reported here is the first of its kind for the use of shape controlled plasmonic nanostructures adsorbed on vertically aligned ZnO NWs for SERS application.

Results and discussion

Fig. 1A shows the SEM image of the AuNR synthesized using seed mediated approach (see experimental for details). Fig. 1B shows an AFM image of the high density of nanorods (~ 100/μm^2) adsorbed onto silicon surface modified with ultrathin (~1 nm) poly(2-vinyl pyridine) (P2VP) layer. The nanorods adsorbed silicon substrate was employed as a planar SERS substrate as discussed later. The inset of the AFM image shows the diameter distribution of the nanorods. The nanorods were found to have a diameter of 15.2 $\pm$0.8 nm and an aspect ratio of nearly three. Fig. 1C shows the UV-vis extinction spectrum of the AuNR in solution, which is characterized by two peaks corresponding to the transverse (~515 nm) and longitudinal (~710 nm) plasmon resonance.

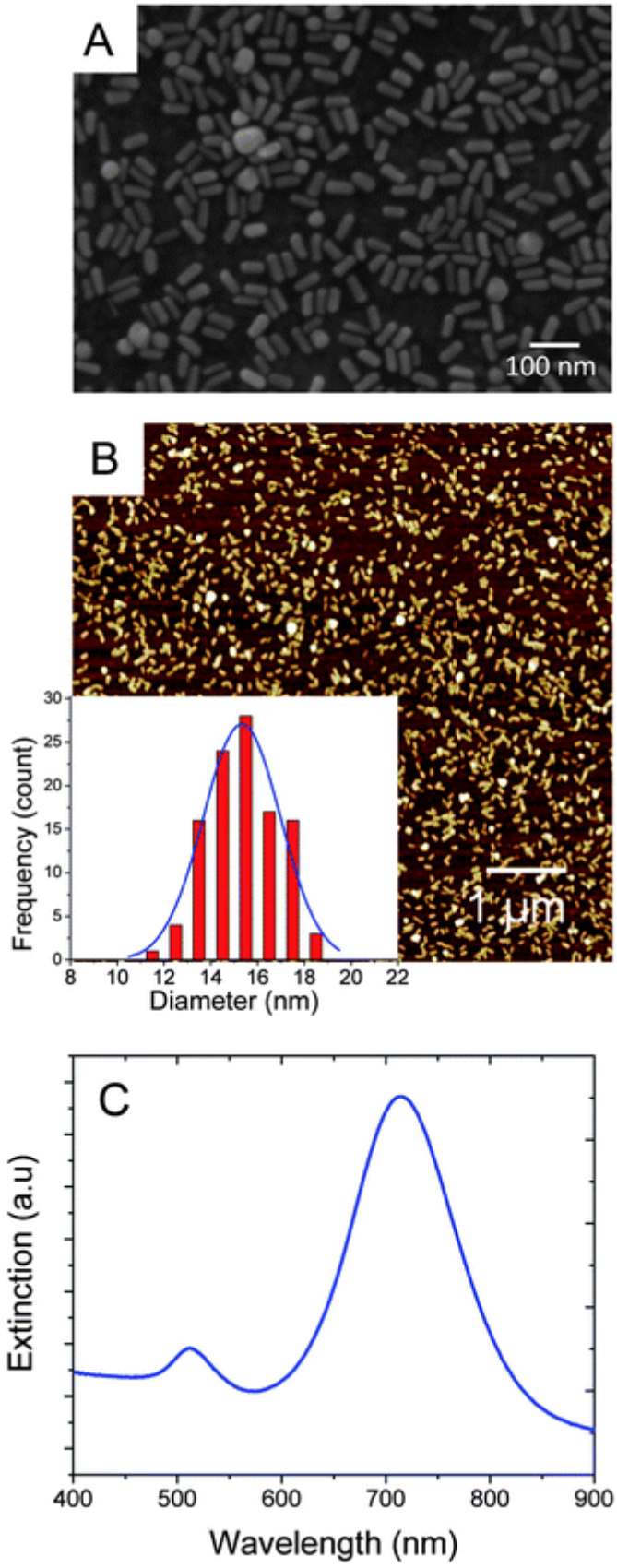

Fig. 1 (A) SEM image showing the aspect ratio of AuNR to be nearly 3.5 (B) AFM image

showing the uniform adsorption of AuNR on P2VP modified Si substrate (Inset: Frequency distribution of the diameter of the AuNR with a Gaussian peak fit showing an average diameter of 15.4 nm) (C) Extinction spectrum of AuNR in solution.

The fabrication of the 3D SERS substrate involves the decoration of vertically aligned ZnO NW with AuNR (or citrate capped gold nanoparticles (AuNP) for comparison) (illustrated in Fig. 2A and B). The process involved the growth of vertically aligned ZnO NWs followed by the surface modification with a thin layer of P2VP. Subsequently, AuNRs were adsorbed on the surface of ZnO NW followed by extensive rinsing with ethanol to remove the weakly bound AuNR. The pyridyl groups of P2VP are known to have high affinity to gold, resulting in strong adsorption of AuNR.[40] Two different control samples were employed to compare the performance of the 3D SERS substrate investigated in this study. The first control sample (called 2D control henceforth) involves a planar silicon substrate adsorbed with a high density of nanorods (see schematic Fig. 2C). Vertically aligned ZnO nanowires coated with a thin layer of gold (~5nm) formed the second control sample (called 3D control henceforth, Fig. 2D).

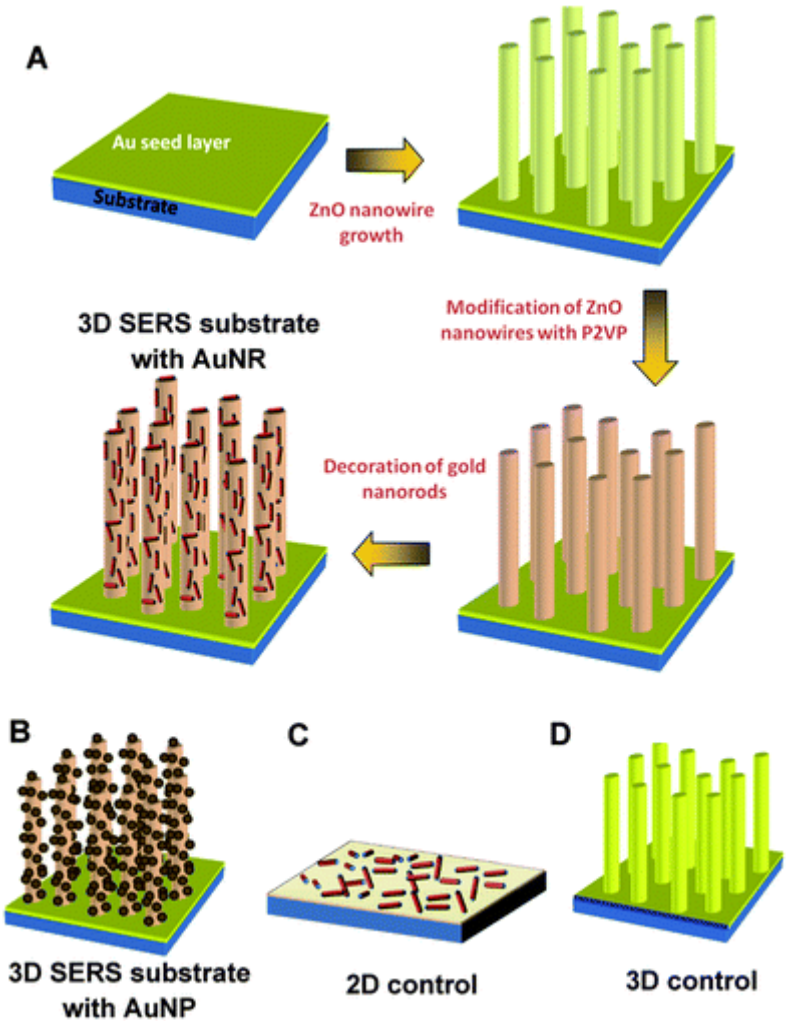

Fig. 2 Schematic showing (A) the fabrication of 3D SERS substrate comprised of vertically aligned ZnO NWs uniformly decorated with AuNR (B) ZnO NWs decorated with AuNP (C) 2D planar control with AuNR adsorbed on silicon substrate (D) 3D control with ZnO NWs coated with 5nm gold layer.

Fig. 3A shows the fluorescence optical micrograph of vertically aligned ZnO nanowires under UV illumination. It is known that ZnO nanowires exhibit two distinct types of photoluminescence (PL) corresponding to the near-UV free-exciton emission (peak at 385 nm) and defect emission (peak at ~510 nm).[41] Using spatially resolved luminescence spectroscopy, it has been

demonstrated that the PL emission occurs primarily at the ZnO wire ends due to the waveguiding nature of the ZnO NWs.[42] Taking advantage of this phenomenon, the alignment of the nanowires can be qualitatively estimated from the optical micrograph. For vertically aligned nanorods, uniform bright PL emission can be observed at the top surface of the nanowires forest, which in fact is the case here. Vertical alignment is further confirmed using SEM imaging as discussed below.

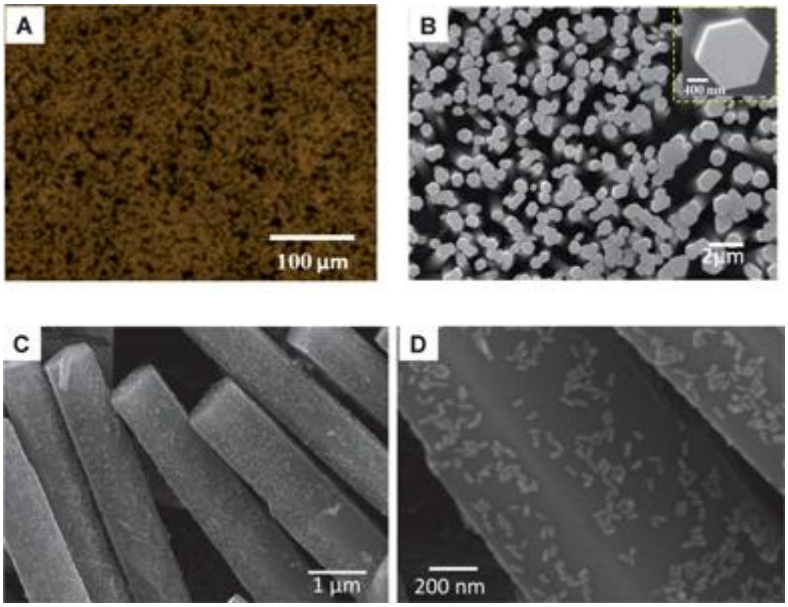

Fig. 3 (A) Fluorescence optical micrograph showing the vertically oriented ZnO NWs. SEM image of (B) vertically aligned pristine ZnO NWs (Inset: High magnification cross sectional view of the (0001) facet) (C) ZnO nanowires uniformly decorated with AuNR along the length of the nanowires (D) Higher magnification image of AuNR adsorbed on the ZnO NWs.

The top view SEM image shows a uniformly aligned nanowire forest with a density of ~7 NW/μm^2 (Fig. 3B). The nanowire forest was found to be mostly comprised of vertically aligned individual nanowires, with occasional fused nanowires. The nanowires exhibited a hexagonal cross section (inset of Fig. 3B) with a height of 6.2 ± 0.8μm and an average cross sectional diameter of 1.1 ± 0.2μm. With the vertically aligned ZnO nanowire forest, the increase in the surface area within the laser footprint was estimated to be nearly 22 times compared to the planar silicon surface. Following the modification of the surface of nanowires with a thin layer of P2VP, the nanowire forest was exposed to AuNR solution, which resulted in the adsorption of the AuNR on the surface of the ZnO nanowires. Fig. 3C shows the side view of the nanowire forest with the nanowires uniformly decorated along the entire length with AuNR. AuNR were also adsorbed on the (0001) facet (top surface) of the ZnO NW. Higher magnification image revealed that the AuNR existed as individual nanorods with occasional dimers and multi-particle aggregates. From numerous SEM images collected at different areas of the substrate, we estimated that ~2000 AuNR were adsorbed on each ZnO NW (surface area of 22 μm^2).

The SERS properties of the 3D SERS substrate comprised of vertically aligned ZnO NW decorated with AuNR was probed using 1,4-benzenedithiol (1,4-BDT) as a model analyte. Due to the distinct Raman fingerprint and the ability to adsorb on gold or silver nanoparticles with thiol linkages, 1,4 BDT was chosen as the model analyte in this study. It is important to note that the use of 1,4 BDT excludes any resonance contribution to the observed SERS enhancement. The Raman spectrum of 1,4 BDT in neat solid state exhibit strong bands at 740, 1058, 1093, 1186 and 1573 cm^{-1}. The prominent band at 1058cm^{-1} corresponds to a combination of phenyl ring breathing mode, CH in-plane bending and CS stretching; 1181cm^{-1} is due to the CH bending and 1573cm^{-1} corresponds to phenyl ring stretching.[43] We utilized the 1573cm^{-1} band to test the detection of trace amounts of 1,4 BDT in ethanol. The SERS substrate (without analyte) does not show any peak in this region.

Fig. 4(A) shows a comparison of the SERS spectra collected from 3D SERS substrates comprised of ZnO NWs decorated with AuNR and AuNP (with 30 nm diameter), 2D and 3D controls following the exposure to 1 mM 1,4-BDT. Raman spectra depicted are an average of six spectra obtained at random locations over 1 × 1 cm^2 area of the substrate. 3D control involves the uniform adsorption of 1,4-BDT over the entire length of nanorods (due to the presence of thin

gold layer), maximizing the number of analyte molecules within the laser footprint. On the other hand, 2D control represents a conventional 2D SERS substrate routinely employed in SERS studies. The intensity of Raman bands observed in the case of 2D control was found to be similar to that obtained from 3D control. On the other hand, SERS spectra from vertically aligned ZnO NWs decorated with AuNR was more than three orders of magnitude higher in intensity compared to 2D and 3D controls and nearly 75 times higher compared to the ZnO NW decorated with AuNP (Fig. 4A). The higher SERS enhancement from ZnO NW decorated with AuNR compared to that obtained from ZnO NW decorated with AuNP is possibly due to the proximity of longitudinal plasmon resonance wavelength of the AuNR to the laser wavelength (785 nm) compared to that of the AuNP. Furthermore, anisotropic shape and sharp corners of gold nanorods result in lightning rod effect (antenna effect), which acts as an additional enhancement factor absent in spherical nanoparticles.[44]

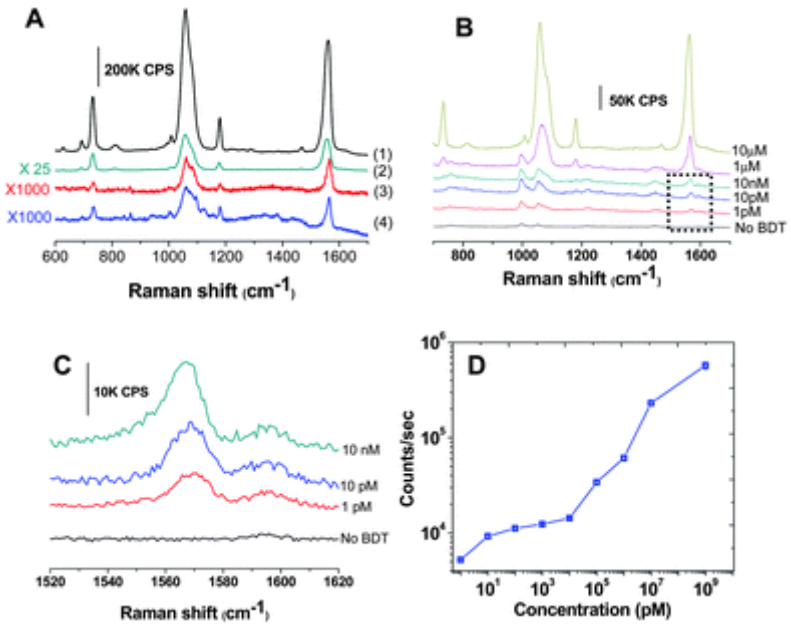

Fig. 4 (A) SERS spectra for 1mM 1,4 BDT adsorbed on (1) ZnO NWs decorated with AuNR, (2) ZnO NWs decorated with AuNP (3) ZnO NWs coated with 5 nm Au film (3D control) and (4) Au NR adsorbed on planar

silicon substrate (2D control) (B) Raman spectra collected from ZnO/AuNR substrate following the exposure to 1,4-BDT at various concentrations (C) High resolution Raman spectra (indicated in B) showing the 1573 cm^{-1} Raman band (D) Concentration *vs.* SERS intensity plot showing the increase in intensity with concentration (error bars within symbols).

The massive enhancement in Raman intensity in the case of the 3D SERS substrate compared to the planar counterpart comes from the dramatically increased number of AuNR within the laser footprint. In the case of the planar SERS substrate, the number of AuNR within the incident laser footprint was found to be 22 ± 2, whereas the 3D SERS substrate was found to have 800 ± 12 AuNR within the laser focal volume. The number of SERS active sites (AuNR) within the laser foot print increased ~ 40 times, which resulted in nearly 3000 times increase in SERS intensity. An additional contribution to the observed high SERS intensity might be from the light reflected multiple times within the interstices of the ZnO NW, thereby additionally interacting with the gold nanorods and further enhancing the Raman intensity.

The SERS enhancement factor (EF) of the 3D substrate was calculated using the intensity of 1567cm^{-1} Raman band using the following expression

$$EF = \frac{I_{SERS}/N_{SERS}}{I_{bulk}/N_{bulk}}$$

Where I and N correspond to the intensity of the Raman band and number of molecules being probed and the subscript refers to SERS and bulk cases. I_{bulk} and N_{bulk} were estimated from the Raman spectra of 100mM of 1,4-BDT in 12M $NaOH_{(aq)}$ solution. The packing density of a

monolayer of 1,4-BDT molecule with a molecular footprint of 0.54nm^2 was calculated to be 1.85 $\times 10^{14}$ molecules/cm^2.[45,46] N_{SERS} was calculated based on a monolayer adsorption of 1,4-BDT on the AuNRs for 1mM concentration, ensuring that the EF is not overestimated. The number of gold nanorods adsorbed on the ZnO NW and subsequently the number of 1,4-BDT molecules was calculated based on a laser spot size of $\sim$530 nm and a focal depth of 2.2 μm. The EF observed for the 3D ZnO SERS substrate with AuNRs adsorbed on them was estimated to be $\sim 3 \times 10^7$.

In order to probe the trace detection ability and limit of detection, the 3D SERS substrates were exposed to lower concentrations of 1,4-BDT (Fig. 4B). Fig. 4(C) shows the 1567.4 cm^{-1} band of 1,4BDT for lower concentrations and in comparison to the SERS substrate with no analyte. It is clear that a concentration of 1pM of 1,4-BDT in ethanol can be easily detected (signal to noise ratio of 6) using the 3D SERS substrate. Fig. 4(D) shows the variation in SERS intensity with concentration of the analyte using a log-log plot showing a monotonic increase in Raman intensity with concentration.

Homogeneity of SERS substrate is extremely critical for reliable quantitative detection of the analytes. In the case of 2D SERS substrate lateral homogeneity is critical, whereas in the case of 3D SERS substrates, an additional degree of homogeneity, namely, vertical homogeneity also becomes critical. In other words, the uniform SERS enhancement at different positions along the length of the nanowires is critical for reliable and repeatable quantitative detection. In order to probe the vertical homogeneity, we performed Z-scan along the length of a single ZnO NW (inset of Fig. 5A). Raman spectra collected along the entire length of the ZnO NWs shows very little variation in the intensity of the Raman bands of the analyte (Fig. 5B). The relative standard deviation (RSD) of the SERS intensity along the length of the nanowire was found to be 5%, which is remarkable considering the simplicity of the fabrication approach demonstrated here. It is important to note that in most of the 3D substrates demonstrated so far, a large variation in the SERS intensity was observed along the length of the templates due to inhomogeneous distribution of the plasmonic nanostructures and/or limited transmission of the incident and scattered light.[47] The excellent vertical homogeneity observed here clearly shows the large focus-tolerance of the 3D SERS substrates owing to the uniform adsorption of the nanorods along the entire length of the nanorods.

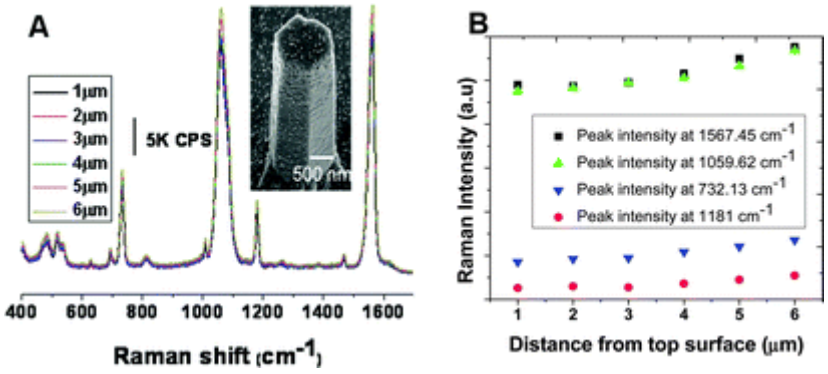

Fig. 5 (A) Average SERS spectra along the length of the ZnO NWs at various distances from the top surface (Inset: High magnification image of the ZnO nanowire from where the Raman intensities were measured.) (B) Plot showing the intensity of the various Raman bands of 1,4 BDT *vs.* distance from the top surface of a single ZnO NW.

Conclusions

In conclusion, we have demonstrated a highly efficient 3D SERS substrate based on vertically aligned ZnO nanowires uniformly decorated with gold nanorods on the surface. The large area ZnO NW-AuNR hybrids fabricated using chemical bath deposition technique at low temperatures is a simple method for the fabrication of highly efficient 3D SERS substrates. The 3D SERS substrates exhibited over three orders of magnitude higher enhancement compared to the 2D counterparts owing to the nearly 40 times higher number of gold nanorods within the laser foot print in conjunction with easy access to analytes to the electromagnetic hotspots. Moreover, the SERS substrate exhibited excellent horizontal and vertical homogeneity (RSD of 5%). These highly active SERS substrates show an enhancement factor of 3×10^{7}, which is remarkable for non-resonant analytes and on par with lithographically defined SERS substrates. We believe that

the optimized version of the SERS substrate demonstrated here by a careful control over the orientation and aggregation of the plasmonic nanostructures on the template nanowires should result in higher enhancements, which can surpass even the best 2D designs in enhancement and homogeneity.

Experimental

AuNR synthesis

AuNRs were synthesized using a seed-mediated approach with some minor modifications.[48,49] Gold seed solution was prepared by sodium borohydride (1mL, 10mM) reduction of 10ml of $HAuCl_4$ (0.25mM) in an aqueous cetyltrimethylammonium bromide (CTAB) (0.1M) solution under continuous magnetic stirring at room temperature. The color of the solution changed from yellow to brown. Growth solution was prepared by mixing together CTAB (95 ml, 0.1 M), silver nitrate (1 ml, 10 mM) and $HAuCl_4$ (5 ml, 10 mM) aqueous solutions. To this solution, ascorbic acid (0.55 ml, 0.1 M) was added and gently stirred to homogenize the solution. Ascorbic acid as a mild reducing agent changes the growth solution from dark yellow to colorless. To the resulting colorless solution, freshly prepared seed solution (0.12 ml) was added and left in the dark for 14 h. The solution turned from colorless to violet brown with most of the color change happening in the first hour. Prior to use, the AuNR solution was centrifuged at 13,000 rpm for 10 min to remove excess CTAB and redispersed in nanopure water (18.2 MΩ-cm). The centrifugation process was repeated twice. Gold nanoparticles with a diameter of ~30 nm have been synthesized according to the procedure discussed in literature, which involved the reduction of gold salt using sodium citrate.[50,51]

Fabrication of 3D SERS substrate

Silicon substrates, cleaned in piranha solution (3 : 1 v/v mixture of H_2SO_4 and 30% H_2O_2), were coated with a 75nm Au layer by thermal evaporation (Edwards 306 thermal evaporator) that was used as a seed layer for the growth of ZnO NW. The root mean square roughness of the gold layer was found to be 1.38 nm over 1 × 1 μm^2. For solution based ZnO NW synthesis, the Au coated Si substrates were floated face-down in a solution containing equimolar (25mM) concentrations of zinc nitrate hexahydrate and hexamethylenetetramine (HMTA) and aged for 6 h at 90 ℃ in a laboratory grade oven box.[52,53] Substrates were subsequently rinsed with water and oven dried at 60 ℃ for 30 min in air. For the decoration of ZnO NW arrays with AuNR, the substrates were

immersed in 1% P2VP solution in ethanol for 1 h and then thoroughly rinsed with ethanol and dried with a stream of nitrogen. Subsequently, the ZnO NW were exposed to AuNR followed by rinsing with water to remove loosely bound AuNRs. SERS measurements were performed by immersing the substrates with the desired concentration of 1,4-BDT in ethanol for 30 min followed by thorough rinsing with ethanol and drying with a stream of nitrogen gas. Different concentrations of 1,4 BDT were prepared by serial dilution of 1mM stock solution.

Planar silicon substrates for comparison (2D control) were fabricated by modifying the silicon substrate with poly(2-vinyl pyridine) (P2VP) by exposing the piranha cleaned silicon surface to 4% P2VP solution in ethanol.[54] After rinsing the silicon substrate with ethanol it was exposed to gold nanorod solution to enable adsorption of the gold nanorods. Finally, the substrate was rinsed with water to remove the loosely bound nanorods leaving a highly dense layer of nanorods on the surface. 3D control samples were prepared by sputtering of 5 nm gold layer on the ZnO NW substrate described above.

UV-vis extinction spectra were collected using a Shimadzu 1800 spectrophotometer. Fluorescence images were obtained with a Leica optical microscope (DM 4000M) using a 50X objective. AFM images were obtained using a Dimension 3000 AFM (Bruker) system in light tapping mode using a silicon nitride cantilever.[55] The thickness of polymer and gold film were measured using scratch test, by scanning along the edge of the scratch made by a sharp scribe. Scanning electron microscope (SEM) images were obtained using a JEOL JSM-7001 FLV field emission SEM at an accelerating voltage of 15kV. Raman spectra were collected using a Renishaw inVia confocal Raman spectrometer mounted on a Leica microscope with 50X objective (NA = 0.90) in the range of 100–3200 cm^{-1} with one accumulation and 10 s exposure time. A 785 nm wavelength diode laser (0.5 mW) was used to excite the sample.

Acknowledgements

The authors thank Prof. Younan Xia from Biomedical Engineering at Washington University for providing access to confocal Raman microscopy system, Dr. Timothy J. Bunning from Air Force Research lab at Wright Patterson Air Force Base for valuable discussions and Dr. Abdennour Abbas at Washington University for technical help. The work was supported by Army Research Office (W81XWH-11-1-0439) and Center for Materials Innovation at Washington University.

References

1 K. Kneipp, Y. Wang, R. R. Dasari and M. S. Feld, *Appl. Spectrosc.*, 1995, **49**, 780–184.

2 S. Nie and S. R. Emory, *Science*, 1997, **275**, 1102–1106.

3 J. A. Dieringer, R. B. Lettan, K. A. Scheidt and R. P. Van Duyne, *J. Am. Chem. Soc.*, 2007, **129**, 16249–16256.

4 M. Mulvihill, A. Tao, K. Benjauthrit, J. Arnold and P. Yang, *Angew. Chem., Int. Ed.*, 2008, **47**, 6456–6460.

5 J. Homola, *Chem. Rev.*, 2008, **108**, 462–493.

6 H. Ko, S. Singamaneni and V. V. Tsukruk, *Small*, 2008, **4**, 1576–1599.

7 M. Quinten, A. Leitner, J. R. Krenn and F. R. Aussenegg, *Opt. Lett.*, 1998, **23**, 1331–1333.

8 S. A. Maier, M. L. Brongersma, P. G. Kik, S. Meltzer, A. A. G. Requicha and H. A. Atwater, *Adv. Mater.*, 2001, **13**, 1501–1505.

9 J. R. Krenn, A. Dereux, J. C. Weeber, E. Bourillot, Y. Lacroute, J. P. Goudonnet, G. Schider, W. Gotschy, A. Leitner, F. R. Aussenegg and C. Girard, *Phys. Rev. Lett.*, 1999, **82**, 2590–2593.

10 S. A. Maier, P. G. Kik and H. A. Atwater, *Appl. Phys. Lett.*, 2002, **81**, 1714–1716.

11 Q.-H. Wei, K.-H. Su, S. Durant and X. Zhang, *Nano Lett.*, 2004, **4**, 1067–1071.

12 J. C. Hulteen and R. P. Van Duyne, *J. Vac. Sci. Technol., A*, 1995, **13**, 1553–1558.

13 J. C. Hulteen, D. A. Treichel, M. T. Smith, M. L. Duval, T. R. Jensen and R. P. Van Duyne, *J. Phys. Chem. B*, 1999, **103**, 3854–3863.

14 C. P. Collier, R. J. Saykally, J. J. Shiang, S. E. Henrichs and J. R. Heath, *Science*, 1998, **277**, 1978–1980.

15 S. Paul, C. Pearson, A. Molloy, M. A. Cousins, M. Green, S. Kolliopoulou, P. Dimitrakis, P. Normand, D. Tsoukalas and M. C. Petty, *Nano Lett.*, 2003, **3**, 533–536.

16 A. Tao, F. Kim, C. Hess, J. Goldberger, R. He, Y. Sun, Y. Xia and P. Yang, *Nano Lett.*, 2003, **3**, 1229–1233.

17 S. Chattopadhyay, H.-C. Lo, C.-H. Hsu, L.-C. Chen and K.-H. Chen, *Chem. Mater.*, 2005, **17**, 553–559.

18 B. Zhang, H. Wang, L. Li, K. Ai, G. Zhang and X. Cheng, *Adv. Funct. Mater.*, 2008, **18**, 2348–2355.

19 S. Deng, H. M. Fan, X. Zhang, K. P. Loh, C.-L. Cheng, C. H. Sow and Y. L. Foo, *Nanotechnology*, 2009, **20**, 175705.

20 C. Cheng, B. Yan, S. M. Wong, X. Li, W. Zhou, T. Yu, Z. Shen, H. Yu and H. J. Fan, *ACS Appl. Mater. Interfaces*, 2010, **2**, 1824–1828.

21 D. M. Kuncicky, B. G. Prevo and O. D. Velev, *J. Mater. Chem.*, 2006, **16**, 1207–1211.

22 S. O. Kucheyev, J. R. Hayes, J. Biener, T. Huser, C. E. Talley and A. V. Hamza, *Appl. Phys. Lett.*, 2006, **89**, 053102.

23 L. H. Qian, X. Q. Yan, T. Fujita, A. Inoue and M. W. Chen, *Appl. Phys. Lett.*, 2007, **90**, 153120.

24 S. Chang, H. Ko, S. Singamaneni, R. Gunawidjaja and V. V. Tsukruk, *Anal. Chem.*, 2009, **81**, 5740–5748.

25 H. Ko, S. Chang and V. V. Tsukruk, *ACS Nano*, 2009, **3**, 181–188.

26 S. Singamaneni, E. Kharlampieva, M. E. McConney, H. Jiang, J.-H. Jang, E. L. Thomas, T. J. Bunning and V. V. Tsukruk, *Adv. Mater.*, 2010, **22**, 1369–1373.

27 T. L. Williamson, X. Guo, A. Zukoski, A. Sood, D. J. Diaz and P. W. Bohn, *J. Phys. Chem. B*, 2005, **109**, 20186–20191.

28 X. Wang, J. H. Song and Z. L. Wang, *J. Mater. Chem.*, 2007, **17**, 711–720.

29 C. Soci, A. Zhang, B. Xiang, S. A. Dayeh, D. P. R. Aplin, J. Park, X. Y. Bao, Y. H. Lo and D. Wang, *Nano Lett.*, 2007, **7**, 1003–1009.

30 X. S. Fang, Y. Bando, U. K. Gautam, C. Ye and D. Goldberg, *J. Mater. Chem.*, 2008, **18**, 509–522.

31 M. A. Khan, T. P. Hogan and B. Shanker, *J. Raman Spectrosc.*, 2009, **40**, 1539–1545.

32 P. Chen, L. Gu, X. Xue, Y. Song, L. Zhu and X. Cao, *Mater. Chem. Phys.*, 2010, **122**, 41–48.

33 L. Chen, L. Luo, Z. Chen, M. Zhang, J. A. Zapien, C. S. Lee and S. T. Lee, *J. Phys. Chem. C*,

2010, **114**, 93–100 .

34 Z. L. Wang, *Mater. Sci. Eng., R*, 2009, **64**, 33–71 .

35 Z. W. Pan, Z. R. Dai and Z. L. Wang, *Science*, 2001, **291**, 1947–1949 .

36 X. Y. Kong, Y. Ding, R. Yang and Z. L. Wang, *Science*, 2004, **303**, 1348–1351 .

37 F. Xu, K. Yu, G. Li, Q. Li and Z. Zhu, *Nanotechnology*, 2006, **17**, 2855 .

38 P. X. Gao and Z. L. Wang, *Appl. Phys. Lett.*, 2004, **84**, 2883–2885 .

39 P. X. Gao and Z. L. Wang, *J. Am. Chem. Soc.*, 2003, **125**, 11299–11305 .

40 S. Malynych, I. Luzinov and G. Chumanov, *J. Phys. Chem. B*, 2002, **106**, 1280–1285 .

41 J. Lee and M. Yoon, *J. Phys. Chem. C*, 2009, **113**, 11952–11958 .

42 S. Ruhle, L. K. van Vugt, H.-Y. Li, N. A. Keizer, L. Kuipers and D. Vanmaekelbergh, *Nano Lett.*, 2008, **8**, 119–123 .

43 S. W. Joo, S. W. Han and K. Kim, *J. Colloid Interface Sci.*, 2001, **240**, 391–399 .

44 R. Boyack and E. C. Le Ru, *Phys. Chem. Chem. Phys.*, 2009, **11**, 7398–7405 .

45 P. H. C. Camargo, C. B. Cobley, M. Rycenga and Y. Xia, *Nanotechnology*, 2009, **20**, 434020 .

46 C. L. Haynes and R. P. Van Duyne, *J. Phys. Chem. B*, 2003, **107**, 7426–7433 .

47 S. Chang, Z. A. Combs, M. K. Gupta, R. Davis and V. V. Tsukruk, *ACS Appl. Mater. Interfaces*, 2010, **2**, 3333–3339 .

48 K. S. Lee and M. A. El-Sayed, *J. Phys. Chem. B*, 2005, **109**, 20331–20338 .

49 A. Gole and C. J. Murphy, *Langmuir*, 2008, **24**, 266–272 .

50 K. C. Grabar, R. G. Freeman, M. B. Hommer and M. J. Natan, *Anal. Chem.*, 1995, **67**, 735–743 .

51 S. Z. Nergiz and S. Singamaneni, *ACS Appl. Mater. Interfaces*, 2011, **3**, 945–951 .

52 L. Vayssieres, *Adv. Mater.*, 2003, **15**, 464–466 .

53 B. Weintraub, S. Chang, S. Singamaneni, W. H. Han, Y. J. Choi, J. Bae, M. Kirkham, V. V. Tsukruk and Y. Deng, *Nanotechnology*, 2008, **19**, 435302 .

54 C. H. Lee, L. Tian and S. Singamaneni, *ACS Appl. Mater. Interfaces*, 2010, **2**, 3429–3425 .

55 M. E. McConney, S. Singamaneni and V. V. Tsukruk, *Polym. Rev.*, 2010, **50**, 235–286 .